AGU PUBLICATIONS

Paleoceanography

RESEARCH ARTICLE
10.1002/2013PA002534

Key Points:
- Tropical Pacific surface and deep ocean temperatures during the Holocene
- Both display significant millennial-scale variability
- Variability probably internal to the climate system

Supporting Information:
- Readme
- Text S1
- Figure S1
- Figure S2
- Figure S3
- Figure S4
- Figure S5
- Table S1

Correspondence to:
D. Khider,
khider@ig.utexas.edu

Citation:
Khider, D., C. S. Jackson, and L. D. Stott (2014), Assessing millennial-scale variability during the Holocene: A perspective from the western tropical Pacific, *Paleoceanography*, *29*, 143–159, doi:10.1002/2013PA002534.

Received 12 JUL 2013
Accepted 17 JAN 2014
Accepted article online 22 JAN 2014
Published online 1 MAR 2014

Assessing millennial-scale variability during the Holocene: A perspective from the western tropical Pacific

D. Khider[1,2], C.S. Jackson[1], and L.D. Stott[2]

[1]Institute for Geophysics, University of Texas at Austin, Austin, Texas, USA, [2]Department of Earth Science, University of Southern California, Los Angeles, California, USA

Abstract We investigate the relationship between tropical Pacific and Southern Ocean variability during the Holocene using the stable oxygen isotope and magnesium/calcium records of cooccurring planktonic and benthic foraminifera from a marine sediment core collected in the western equatorial Pacific. The planktonic record exhibits millennial-scale sea surface temperature (SST) oscillations over the Holocene of ~0.5°C while the benthic $\delta^{18}O_c$ document ~0.10‰ millennial-scale changes of Upper Circumpolar Deep Water (UCDW), a water mass which outcrops in the Southern Ocean. Solar forcing as an explanation for millennial-scale SST variability requires (1) a large climate sensitivity and (2) a long 400 year delayed response, suggesting that if solar forcing is the cause of the variability, it would need to be considerably amplified by processes within the climate system at least at the core location. We also explore the possibility that SST variability arose from volcanic forcing using a simple red noise model. Our best estimates of volcanic forcing falls short of reproducing the amplitude of observed SST variations although it produces power at low-frequency similar to that observed in the MD81 record. Although we cannot totally discount the volcanic and solar forcing hypotheses, we are left to consider that the most plausible source for Holocene millennial-scale variability lies within the climate system itself. In particular, UCDW variability coincided with deep North Atlantic changes, indicating a role for the deep ocean in Holocene millennial-scale variability.

1. Introduction

In contrast to the well-documented climatic changes that characterized the last glacial and deglacial periods, the Earth's climate during the Holocene has often been characterized as comparatively more stable. This view is being challenged now by studies that document climate changes during the past 10,000 years, some of which appear to have been abrupt, albeit of smaller amplitude than their glacial counterparts. Indeed, centennial- to millennial-scale variability has now been identified in a number of Holocene climate archives [e.g., *Bianchi and McCave*, 1999; *deMenocal et al*., 2000; *Jansen et al*., 2007; *Mayewski et al*., 2004; *O'Brien et al*., 1995; *Viau et al*., 2002; *Wang et al*., 2005]. Examples of such variability include the 8.2 kyr event, and the Medieval Climate Anomaly/Little Ice Age of the past 1000 years. But the identification of climate variations during the Holocene poses an important question; in the absence of large CO_2 variations [*Monnin et al*., 2001], does the Earth's climate system respond to relatively small changes in external forcing [*Bond et al*., 1997, 2001] or, is there an internal driver that causes these millennial-scale changes? And, is there a natural recurrence frequency of climate variability during the Holocene? A number of individual paleoclimate records have supported the existence of semiperiodic, regional-scale climate variability. But it has been difficult to assess whether or not these regional patterns are part of a coherent global climate response [*Jansen et al*., 2007].

A correlation has been found between solar activity, derived from cosmogenic isotope records and paleoclimate proxies that suggests changes in insolation may have been a contributing influence to millennial-scale climate variations on ~1000 and ~2500 year timescales during the Holocene [e.g., *Bond et al*., 2001; *Debret et al*., 2007, 2009; *Polissar et al*., 2006; *Wang et al*., 2005]. However, a mechanism by which small changes in total solar irradiance can influence a global climate response is not currently known [*Haigh*, 2001, 2007]. Numerical models have shown that tropical ocean/atmosphere dynamics is sensitive to small sea surface temperature (SST) changes within the Indo-Pacific Warm Pool (IPWP) [*Jochum and Potemra*, 2008; *McBride et al*., 2003; *Neale and Slingo*, 2003; *Qu et al*., 2005], which constitutes the largest reservoir of ocean heat content. Furthermore, SST changes within IPWP resembled Northern Hemisphere temperature

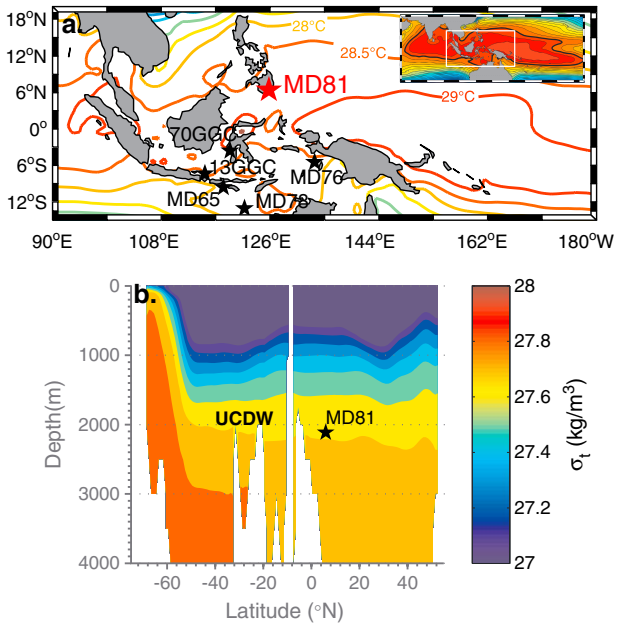

Figure 1. Oceanographic Settings. (a) Location of core MD98-2181 (red star) on a map of mean annual sea surface temperatures inferred from the World Ocean Atlas 09 [*Locarnini et al.*, 2010]. The location of other high-resolution Holocene sedimentary records are shown in black (MD98-2176 [*Stott et al.*, 2004], MD98-2165 [*Levi et al.*, 2007], MD0123-78 [*Xu et al.*, 2008], BJ8-03-70GGC, and BJ8-03-13GGC [*Linsley et al.*, 2010]). (b) Potential density (estimated from temperature and salinity data extracted from the World Ocean Atlas 09 [*Antonov et al.*, 2010; *Locarnini et al.*, 2010]) of the Pacific Ocean along a North-South transect centered around 160°E. The location of MD81 is marked by a star. The core site is bathed by Upper Circumpolar Deep Water (UCDW), which outcrops in the Southern Ocean.

variations over the last 2000 years [*Newton et al.*, 2006; *Oppo et al.*, 2009] and also during the last glacial period [*Dannenmann et al.*, 2003; *Saikku et al.*, 2009; *Stott et al.*, 2002], suggesting the IPWP and high latitudes are coupled through both atmospheric and oceanic links [*Cane*, 1998].

While solar forcing may be one of the influences on Earth's climate variability, there exists the possibility that the oceans themselves can drive some of the millennial-scale variability observed in proxy records. [*Debret et al.*, 2007, 2009] identified a ~1500 year periodicity in Holocene records from the Atlantic, which could not be attributed to solar forcing, but rather were interpreted to reflect internal modes of ocean/atmosphere interactions. For instance, internal modes of variability may be linked to deep ocean circulation changes [*Bianchi and McCave*, 1999; *Broecker*, 2000, 2001; *Denton and Broecker*, 2008; *Oppo et al.*, 2003]. However, the proxy records from which these ocean influences have been inferred have focused mostly on the North Atlantic and variations in the strength of the North Atlantic Overturning Circulation. Additional well-dated, high-resolution archives of Southern Ocean variability are needed to better address whether or not small changes in the strength of the Atlantic Meridional Overturning Circulation may influence the entire ocean/atmosphere system on millennial timescales.

There are a number of marine sediment cores from the IPWP that have sufficient temporal resolution to allow for an evaluation of Holocene tropical SST variability and its relationship to solar forcing and high-latitude climate variability [*Levi et al.*, 2007; *Linsley et al.*, 2010; *Stott et al.*, 2004; *Xu et al.*, 2008, Figure 1]. But one of the main challenges in attributing Holocene millennial-scale variability is the poor chronologic constraints inherent to marine sediment cores, which are necessary for intersite comparisons. In the present study we have attempted to circumvent this problem by analyzing the geochemical composition of cooccurring benthic and planktonic foraminifera from a single sediment core [*Stott et al.*, 2007] collected in the Davao Gulf at the edge of the western Pacific Warm Pool (MD98-2181, hereafter MD81, 6.45°N, 125.83°E, 2114 m water depth, Figure 1). The oxygen isotopic composition ($\delta^{18}O_c$) and trace element chemistry (Mg/Ca) of planktonic foraminifera from this core document SST and $\delta^{18}O_{sw}$ variability within the IPWP. The benthic foraminifera $\delta^{18}O_c$ from the same samples provides a record of deep ocean temperature and salinities. And because these conservative deep water properties are acquired in the Southern Ocean, the MD81 benthic $\delta^{18}O_c$ is a record of high southern latitude variability. Thus, MD81 allows us to investigate the relative timing of tropical and high southern latitude variability from a single location, circumventing the problem of intersite chronologic uncertainties. A time series analysis of the MD81 sedimentary record allows us to (1) identify periodicities in western tropical Pacific SSTs and Southern Ocean temperature and salinity variations, (2) investigate the relative timing of tropical SST and Southern Ocean variability, and (3) investigate the relationship between changes in total solar irradiance (TSI) and tropical Pacific SST variability. These time series analyses allow us to infer whether small changes in TSI had an impact on tropical SSTs. Given the importance of the IPWP to the global atmospheric and oceanic circulation [*Qu et al.*, 2005], assessing the magnitude of IPWP SSTs response to changes in solar irradiance may help elucidate a feedback mechanism through which small changes in TSI

can affect a global climate response. We also investigate the timing of Southern Ocean temperature variability and North Atlantic deep water variability during the Holocene [*Hoogakker et al*., 2011; *Oppo et al*., 2003; *Thornalley et al*., 2009]. From this we evaluate whether or not changes in the deep ocean circulation could have influenced the global climate variability during the Holocene. Finally, we investigate the alternate hypothesis that Holocene millennial-scale variability is forced by volcanic eruptions.

2. Regional Oceanography

Marine sediment core MD81 (Figure 1) was collected as part of the IMAGES program using the R/V *Marion Dufresne*. The core location is the Davao Gulf, south of Mindanao (6.45°N, 125.83°E, 2114 m), on the edge of the western Pacific warm pool. Surface ocean variability at our study site is strongly influenced by the position of the zone of maximum solar insolation, the monsoons, and El Niño–Southern Oscillation (ENSO) on seasonal and interannual timescales [*Gordon*, 2005]. The mean annual SST near the MD81 site is 28.5°C (World Ocean Atlas 09 [*Locarnini et al*., 2010]). SSTs are coldest during boreal winter (January–March, 27.7°C) [*Locarnini et al*., 2010] and warmest during the summer months (July–September (JAS), 29°C) [*Locarnini et al*., 2010]. Mean annual sea surface salinity (SSS) at the study site is 34.1 psu [*Antonov et al*., 2010]. The seasonal salinity cycle (~0.3 psu) reflects changes in precipitation that accompanies the seasonal migration of the deep atmospheric convection zone, with lower salinity in boreal summer (JAS, 34 psu, [*Antonov et al*., 2010]) and higher salinity in boreal winter (December–February, 34.3 psu) [*Antonov et al*., 2010]. SSS anomalies associated with moderate to strong El Niño (La Niña) are 0.15 ± 0.13 psu (-0.20 ± 0.11 psu), estimated from the Simple Ocean Data Assimilation reanalysis data set [*Carton and Giese*, 2008]. A year was defined from May to the following April in order to accentuate the seasonal locking of ENSO. Moderate to strong events were selected based on the NOAA consensus list of El Niño and La Niña events (http://ggweather.com/enso/oni.htm). The SSS anomalies during El Niño are associated with a reduction in precipitation over the Maritime Continent.

At 2114 m, the MD81 site is bathed by Upper Circumpolar Deep Water (UCDW) [*Saikku et al*., 2009; *Stott et al*., 2007]. Circumpolar Deep Water (CDW) forms in the Antarctic Circumpolar Current, where North Atlantic Deep Water (NADW) mixes with recirculated deep water from the Indian and Pacific Oceans. The main export pathway for CDW to the Pacific Ocean is the Deep Western Boundary Current [*van de Flierdt et al*., 2004]. This water mass travels northward into the Pacific Ocean along the Tonga-Karmadec trench and up the western Pacific island arc before turning clockwise north of the equator to fill the deep North Pacific. The water mass is further modified and returns southward at 2–3 km depth as UCDW, characterized by potential density of 27.4–28.0 kg/m^3 [*Rintoul et al*., 2001]. Therefore, deep ocean properties at the MD81 site vary in response to Southern Ocean changes and cooccurring planktonic and benthic foraminifera from this single location allows the investigation of the relationship between tropical and southern high-latitude variability over the Holocene, assuming that the deep water transit time from the formation region in the Southern Ocean to the MD81 site is taken into account (section 3.2.).

3. Methods

3.1. Age Model

The age model for MD81 is based on 14 ^{14}C ages of *Globigerinoides sacculifer*, mixed *G. sacculifer* with *G. ruber*, or mixed planktonics (Table S1 in the supporting information) calibrated to calendar years using the Marine09 calibration curve [*Reimer et al*., 2009]. The modern reservoir age correction ($\pm 1\sigma$) has been estimated at 5 ± 50 years in Guam [*Southon et al*., 2002], 34 ± 44 and 168 ± 43 in Palau [*Yoneda et al*., 2007], and 6 ± 42 in Ponape, Micronesia [*Yoneda et al*., 2007]. We apply a reservoir age correction for this study of 15 ± 79 years. The quoted 1σ uncertainty represents the analytical uncertainty in the ^{14}C measurements and the spatial heterogeneity in the estimates of the modern reservoir age correction. There is ^{14}C data from Papua New Guinea corals that suggests a reduction in the marine reservoir age in the mid-Holocene [*McGregor et al*., 2008]. But a history of varying reservoir ages throughout the Holocene is unavailable, and therefore, there is no way to evaluate whether varying reservoir corrections should be applied. Thus, we have applied a constant reservoir age correction for each of the ^{14}C ages in this study. For each ^{14}C age a calendar age is drawn from a normal distribution with mean $\mu = (\text{measured } ^{14}\text{C age} + \Delta R)$ and standard deviation $\sigma = (\sigma_{\text{analytical}}{}^2 + \sigma_{\Delta R}{}^2)^{1/2}$, where $\sigma_{\text{analytical}}$ represents the uncertainty in the measured ^{14}C and $\sigma_{\Delta R} = 79$ years represents the uncertainty in the reservoir age. We then calibrate this ^{14}C age distribution

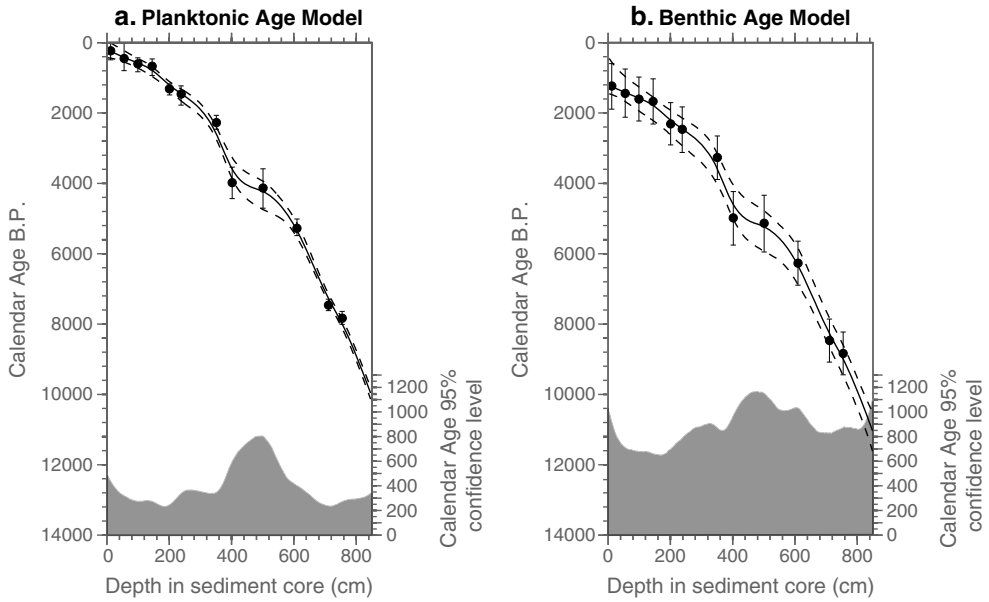

Figure 2. Age model for core MD98-2181. (a) Planktonic age model. The filled circles represent the planktonic mean calibrated ages obtained from *G. sacculifer*, a mixture of *G. sacculifer/G. ruber*, and mixed planktonic species. The solid line represents the constructed age model using a smoothing cubic spline interpolation scheme, with the 95% confidence level from Monte-Carlo simulations represented by the dotted lines and the shaded area. (b) Benthic age model. The filled circles represent the benthic mean calibrated age obtained from adding 1000 ± 300 years to the planktonic age distributions. The solid line represents the constructed age model using a smoothing cubic spline interpolation scheme, with the 95% confidence level from Monte-Carlo simulations represented by the dotted lines and the shaded area.

against the Marine09 curve [*Reimer et al.*, 2009]. In order to take into account the error in the Marine09 calibration, we use a Monte Carlo process ($n = 10{,}000$) in which each ^{14}C age within the distribution is calibrated against a random rendition of the Marine09 curve, created assuming a normally distributed error around the mean value.

The resulting calendar age distributions are then used to construct the age model for MD81 by using the mean of the distribution at each ^{14}C horizon and a smoothing spline interpolation scheme (Figure 2a). The 95% confidence envelope for the MD81 age model is estimated through Monte Carlo trials, in which age models are constructed by selecting tie points from the inferred calendar age distributions and using a smoothing spline interpolation scheme. This Monte Carlo process may result in age reversal between ^{14}C horizons. Although age model reversals are possible through bioturbation, we removed all age models that would result in stratigraphic reversals. The number of Monte Carlo trials was set to obtain 10,000 independent age models to estimate the 95% confidence interval at each horizon in the MD81 core. The age-depth plot (Figure 2) shows a continuous sediment accumulation though the Holocene, with higher accumulation rate in the late Holocene (~180 cm/kyr) compared to the early Holocene (~80 cm/kyr), although this may be an artifact of deformation from the CALYPSO coring system [*Skinner and McCave*, 2003].

3.2. Planktonic/Benthic Age Offset

In order to compare the timing of tropical and deep ocean variability, the deep water transit time from the formation region in the Southern Ocean to the MD81 site needs to be taken into account. Although ^{14}C is not a pure water mass tracer as it is subjected to interior mixing, the present-day propagation time between the Southern Ocean and the tropical Pacific can be estimated from the prebomb ^{14}C distributions of dissolved inorganic carbon in the Pacific using the Global Ocean Data Analysis Project (GLODAP) [*Key et al.*, 2004] database. The reservoir age of subpolar surface waters, the source of CDW, has been estimated at 560 ± 40 years [*Sikes et al.*, 2000, Figure 4]. Modern deep water age at the MD81 age is ~1500 years (Figure 3), suggesting a ~1000 years propagation time between the Southern Ocean to the MD81 site. This estimate of the average transit time is further verified by analysis of the ^{14}C ages of cooccurring planktonic and benthic foraminifera (Figure 3). The Holocene transit time averages 1040 ± 47 and ranges from 470 ± 151 to 1590 ± 71 years (Figure 3

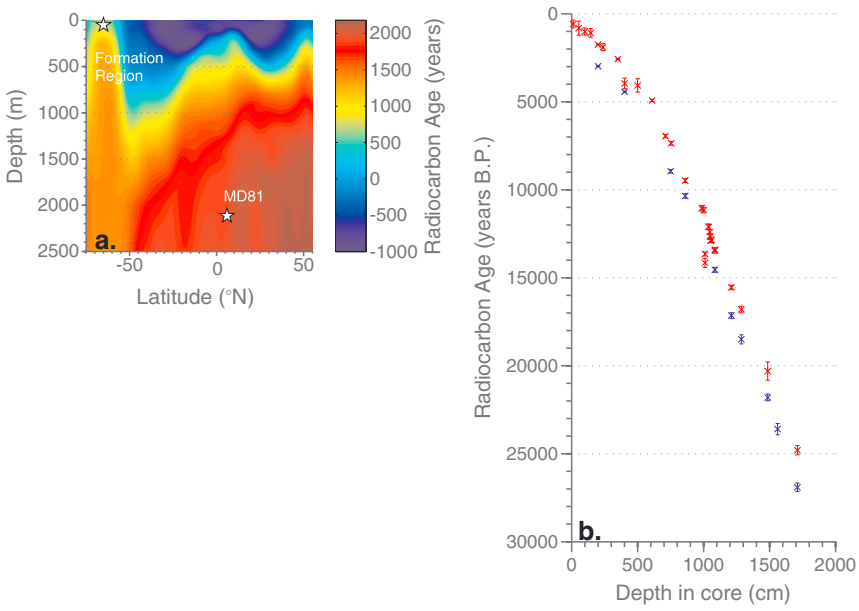

Figure 3. Planktonic-Benthic Offset (a) Modern radiocarbon age (estimated from GLODAP $\Delta^{14}C$) of the Pacific Ocean along a North-South transect centered at 160°E. The location of MD81 and the formation region of UCDW are marked by white stars. (b) Planktonic (red) and benthic (blue) radiocarbon ages for core MD81 for the Holocene (this study, Table S1 in the supporting information) and the deglacial [*Stott et al*., 2007]. The vertical error bars represent the 2σ uncertainty on the radiocarbon measurements.

and Table S1 in the supporting information). Here the quoted uncertainty represents the analytical uncertainty in the ^{14}C measurements, while the range represents changes in transit time and is therefore a better estimate of the total uncertainty in the planktonic-benthic offset. Therefore, we assume a 1000 ± 300 (1σ uncertainty) years offset between the planktonic and benthic data following previous studies [*Saikku et al*., 2009; *Stott et al*., 2007]. When the planktonic and benthic records are then compared, the benthic data is a reflection of what the temperature and salinity was in the Southern Ocean at the time the tropical surface water signal was generated.

To obtain an independent age model for the MD81 benthic data, we adjusted each tie point in the planktonic calendar age distributions using a normal distribution characterized by a mean of 1000 years and a standard deviation of 300 years. The benthic age model was then obtained by using the mean of the adjusted distribution at each ^{14}C horizon and a smoothing spline interpolation scheme (Figure 2b). To verify that the Monte Carlo series has converged, we checked that the mean offset between the planktonic and benthic age models was ~1000 years at each ^{14}C horizon. The 95% confidence envelope for the MD81 benthic age model is estimated through Monte Carlo trials ($n = 10{,}000$), in which age models are constructed by selecting tie points from the inferred adjusted age distributions and using a smoothing spline interpolation scheme.

3.3. Analytical Techniques

For this study, MD81 was sampled at 2 cm intervals for the section corresponding to the Holocene. The bulk sediment samples were disaggregated in a sodium hexametaphosphate solution and wet-sieved through a 63 μm mesh to remove the clay fraction. The >63 μm fraction was then dry-sieved at >180 μm. Approximately 50–100 specimens of the planktonic foraminifer *G. ruber* (white, sensu stricto and sensu lato) and 5–20 specimens of the epifaunal benthic foraminifer *Cibicidoides mundulus* were picked from the >180 μm fraction under a binocular microscope. The foraminifera were then cleaned following a protocol adapted from *Barker et al*. [2003] [*Saikku et al*., 2009]. The calcite preservation in MD81 samples is excellent because the core was taken above the present-day lysocline and is characterized by high accumulation rates.

The $\delta^{18}O_c$ values were measured using a Multiprep Dual Inlet system attached to an Isoprime stable isotope ratio mass spectrometer housed at the University of Southern California. Each sequential run included 30–50 foraminiferal samples together with 10–15 calcite standards (University of Southern California (USC) Ultissima marble) used to monitor analytical precision. The long-term precision of the Ultissima standard $\delta^{18}O$ values

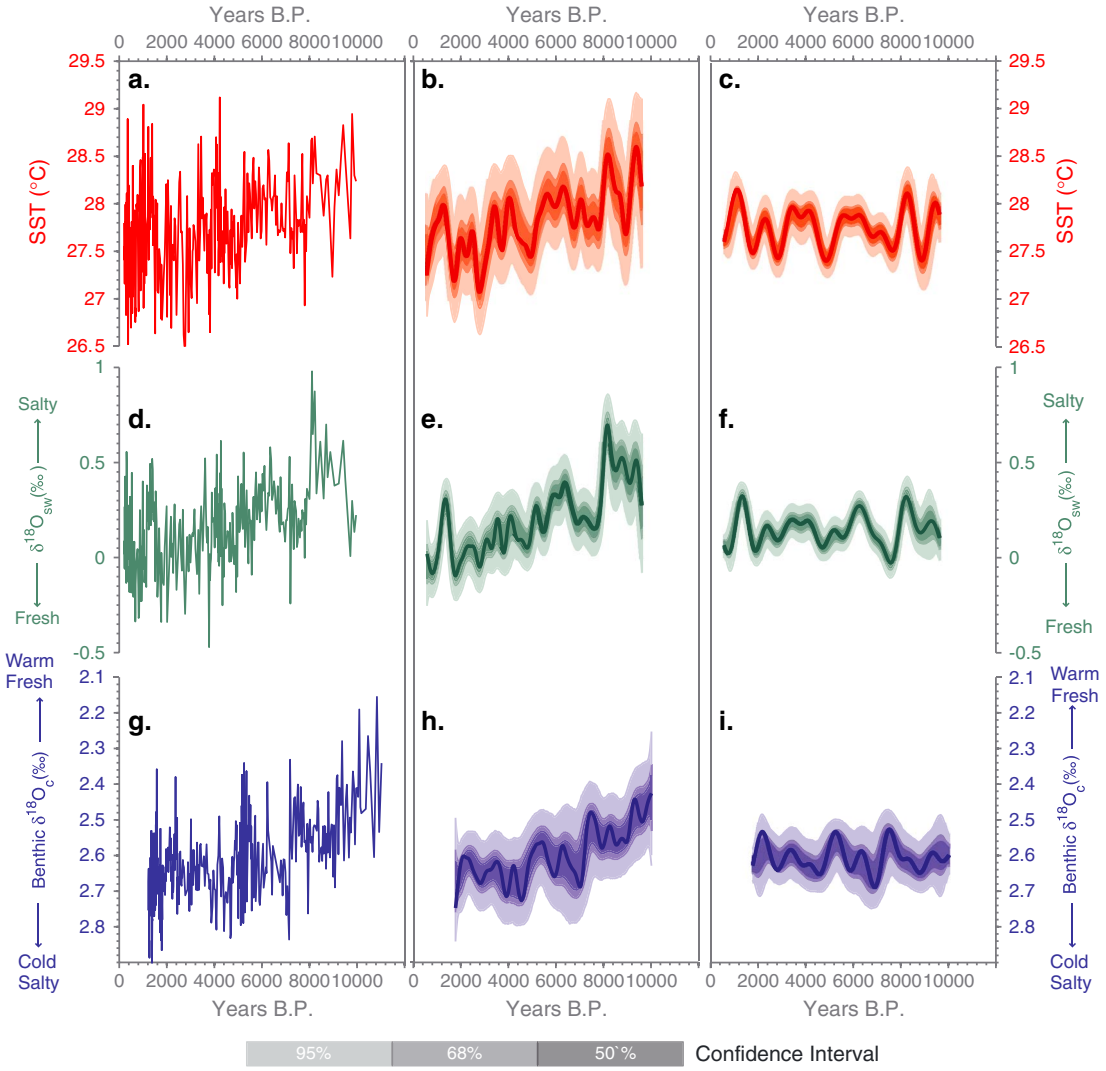

Figure 4. Holocene MD98-2181 Planktonic and Benthic records. (a) Sea Surface Temperature over the Holocene in the Davao Gulf inferred from G. ruber Mg/Ca. (b) A 500 year low-pass filter. The thick line represents the 500 year low-pass filtered SST while the shaded areas represent the 50%, 68%, and 90% confidence intervals. (c) A 900–3000 year band-pass filter. The thick line represents the 900–3000 year band pass filtered SST while the shaded areas represent the 50%, 68%, and 90% confidence intervals. (d–f) Same as Figures 4a–4c but for $\delta^{18}O_{sw}$ inferred from G. ruber $T_{Mg/Ca}$ and $\delta^{18}O_c$. The record has been corrected for ice volume effect. (g–i) Same as Figures 4a–4c but for the benthic $\delta^{18}O_c$ record, which represents UCDW variability. The record has been corrected for ice volume effect. The uncertainty on the low-pass and band-pass filters was estimated for the common length of the age model as extrapolation would bias the uncertainty estimates. Also note that the error is not necessarily normally distributed around the original time series, a reflection of the fact that age models resulting in stratigraphic reversals were not considered in this study. The records are presented on the same *y* axis to highlight the contribution of millennial-scale variability to the Holocene record.

measured during this study was 0.08‰. The precision on replicate analyses is 0.14‰ for *G. ruber* and *C. mundulus* samples. For Mg/Ca analysis, the foraminiferal samples were dissolved in 500 µL of 5% nitric acid solution and analyzed on a Jobin Yvon inductively coupled plasma atomic emission spectrometer housed at USC. Each sample measurement was bracketed by a standard solution made from solid Mg and reagent grade $CaCO_3$ in an elemental ratio of 5.63 mmol/mol, used to adjust the foraminiferal sample Mg/Ca for instrument drift. The nominal precision of the instrument is 0.1 mmol/mol determined from replicate analyses of standards. The precision on G. ruber samples is 0.2 mmol/mol. Fe/Ca and Mn/Ca ratios were used to monitor potential silicate contamination [*Barker et al.*, 2003]. The Mg/Ca ratios were converted to temperature using $Mg/Ca = 0.45\exp(0.09\,T)$, which is derived from the culturing experiment (temperature only) of *Kisakürek et al.* [2008] for the planktonic foraminifer G. ruber. This equation is equivalent to the more traditionally used *Anand et al.* [2003] equation. The motivation for using this equation based on the data of

Kisakürek et al. [2008] stems from our approach to uncertainty quantification, which is detailed in the following section and in Text S1 in the supporting information. We also calculated the stable oxygen isotopic composition of seawater ($\delta^{18}O_{sw}$) from the measured $\delta^{18}O_c$ and the Mg/Ca-estimated SST using the *Bemis et al*. [1998] high-light equation for Orbulina universa: $T = 14.9 - 4.8(\delta_c - \delta_{sw} + 0.27)$.

3.4. Uncertainty Estimation

Paleoceanographic studies present a unique challenge for the estimation of uncertainty in the reconstructed parameters since both errors in abscissa (age model) and ordinates (the reconstructed parameter) need to be taken into account. The most traditional approach has been to report the error associated with the age model and the variable being reconstructed separately, which may over/underestimate the actual error associated with the reconstruction since it does not take into account the time sampling of the data. Here we use a Monte Carlo process to assess the uncertainty envelope on the SST, $\delta^{18}O_{sw}$, and $\delta^{18}O_c$ estimates of variability on millennial timescales.

We considered two sources of uncertainty in the SST and $\delta^{18}O_{sw}$ estimates: the analytical uncertainty on the Mg/Ca and $\delta^{18}O_c$, which we assumed to be normally distributed and independent from sample to sample, and the uncertainty on the calibration equation, which would affect a group of measurements similarly (i.e., only one equation is used to obtain SST for the entire record). We combined both sources of uncertainty in the Monte-Carlo simulations ($n = 10{,}000$) of the SST and $\delta^{18}O_{sw}$ records. For each Monte Carlo trial, Mg/Ca and $\delta^{18}O_c$ estimates at each horizon were varied in normal distributions defined by their analytical uncertainty ($1\sigma = 0.2$ mmol/mol in Mg/Ca and $1\sigma = 0.14$‰ in $\delta^{18}O_c$). Each complete Mg/Ca and $\delta^{18}O_c$ record for the Holocene was then transformed into SST and $\delta^{18}O_{sw}$ estimates using a possible solution for the calibration equations. To do so, we use a Bayesian approach to enumerate all the possible solutions for the calibration equations. Bayesian statistics employs algorithms to draw a set of samples (in this case, the coefficients of the calibration equation) from prior probability distributions and update the probability of the set of parameters in light of the current data [*Bolstad*, 2010]. The characteristics of the prior distribution are determined by information available before the current data has been analyzed [*Wilks*, 2011]. Bayes' theorem then combines the prior density distribution and the current data in the posterior probability distribution of the parameter, which measures how plausible the prior value of the parameter is after we have observed the data [*Bolstad*, 2010]. A detail description of the Bayesian calculation and a comparison to the more traditional least squares method is provided in Text S1 in the supporting information.

These SST and $\delta^{18}O_{sw}$ records were then put on an age scale using the age models generated previously through Monte Carlo trials. This process generated 10,000 renditions of the SST and $\delta^{18}O_{sw}$ records. The average uncertainty (2σ) on the SST and $\delta^{18}O_{sw}$ is 1.1°C and 0.37‰, respectively. The quoted uncertainty takes into account only the analytical and calibration errors but does not account for additional biases on the Mg/Ca thermometer such as changes in deep-ocean ΔCO_3^{2} [*Dekens et al*., 2002; *Regenberg et al*., 2006], salinity [*Arbuszewski et al*., 2010; *Mathien-Blard and Bassinot*, 2009], or changes in the seasonality of G. ruber. Because the focus of this study is on the millennial timescale, we also evaluated the uncertainty in the 500 year low-pass filtered record. To do so, we applied a 500 year low-pass filter to each simulation ($n = 1{,}0000$) and estimated the confidence levels on SST and $\delta^{18}O_{sw}$ estimates from the resulting distributions. We used a similar approach (analytical uncertainty only) to estimate the uncertainty on the benthic $\delta^{18}O_c$ curve.

3.5. Spectral Analysis

To investigate the characteristic timescale(s) of surface and deep ocean variability, we performed spectral analysis on the SST, $\delta^{18}O_{sw}$, and benthic $\delta^{18}O_c$ records. Paleoclimate studies often result in time series with nonuniform sampling in the time domain. However, most of the method employed in spectral analyses [*Ghil et al*., 2002] require evenly spaced time series and we would therefore need a step to interpolate our original time series so that the data are evenly spaced. Because the interpolated data points are no longer independent, such an interpolation scheme could bias the statistical results [*Schulz and Stattegger*, 1997; *Schulz and Mudelsee*, 2002] and enhance the low-frequency components at the expense of the high-frequency components, leading to a reddening of the spectrum compared to the true spectrum [*Schulz and Stattegger*, 1997]. Here we use the Lomb-Scargle Fourier Transform [*Lomb*, 1976; *Scargle*, 1982, 1989] in combination with a Welch-Overlapped-Segment-Averaging (WOSA) procedure for consistent spectral estimates [*Schulz and*

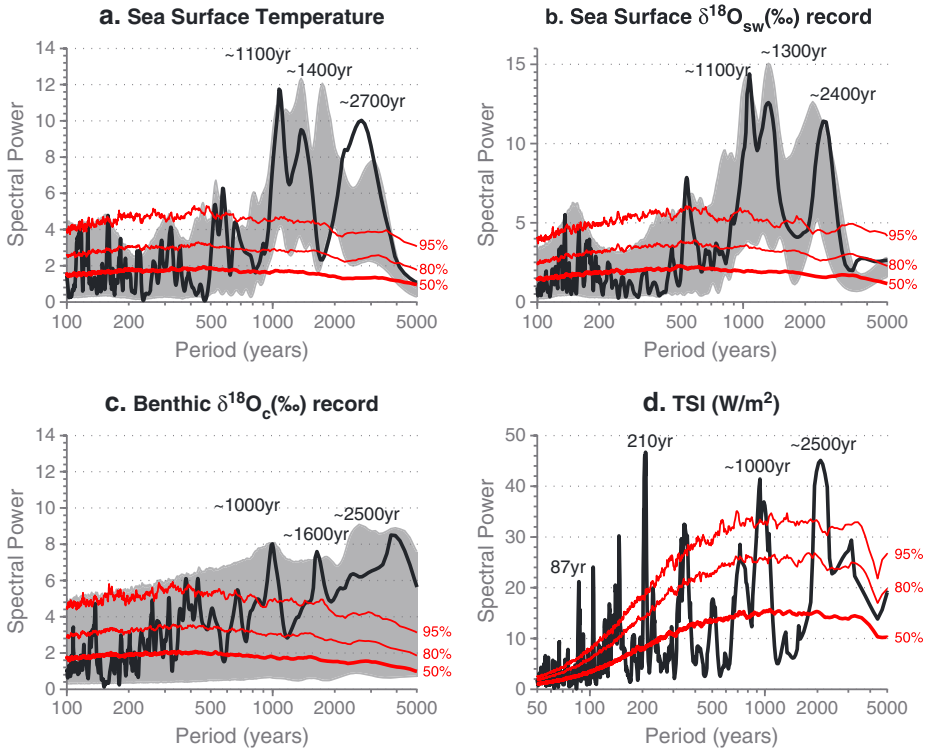

Figure 5. Spectral analysis. (a) Lomb-Scargle periodogram for the SST record. The red lines represent the 50%, 80%, and 95% ensemble of the red noise (AR1) models. The AR1 models were generated using a characteristic timescale $T = 11.3$ years obtained from TAUEST [*Mudelsee*, 2002]. The shaded area represents the 95% confidence envelope for the periodogram based on the 10,000 Monte-Carlo simulations. (b) Same as Figure 5a but for the $\delta^{18}O_{sw}$ record. The characteristic timescale is $T = 15.9$ years. (c) Same as Figure 5a but for the benthic $\delta^{18}O_c$ record. The characteristic timescale is $T = 9.5$ years. (d) Same as Figure 5a but for the solar variability (TSI) record of *Steinhilber et al.* [2009]. The characteristic timescale is $T = 30.2$ years.

Stattegger, 1997; *Welch*, 1967]. This method weights the data on a "per point" basis instead of a "per time interval" basis. For a set of n data points $\{y_j\}$ at time $\{t_j\}$ (with $j = 1,2,..,n$), not necessarily uniformly spaced, the normalized Lomb-Scargle periodogram, $P(\omega)$ at angular frequency $\omega = 2\pi f > 0$ is:

$$P(\omega) = \frac{1}{2\sigma^2}\left[\frac{\left(\sum_{j=1}^{n}\left(y_j-\bar{y}\right)\cos\omega\left(t_j-\tau\right)\right)^2}{\sum_{j=1}^{n}\cos^2\omega\left(t_j-\tau\right)} + \frac{\left(\sum_{j=1}^{n}\left(y_j-\bar{y}\right)\sin\omega\left(t_j-\tau\right)\right)^2}{\sum_{j=1}^{n}\sin^2\omega\left(t_j-\tau\right)}\right]$$

where $\bar{y}$ and σ^2 are the mean and the variance of the $\{y_j\}$. The constant τ is an offset that makes $P(\omega)$ independent of shifting the t_j's by any constant and is defined as follows:

$$\tan(2\omega\tau) = \frac{\sum_{j=1}^{n}\sin\left(2\omega t_j\right)}{\sum_{j=1}^{n}\cos\left(2\omega t_j\right)}$$

Prior to spectral analysis, the time series was detrended using a first- or second-order polynomial and standardized (mean = 0, standard deviation = 1). The time series was then divided into 3 overlapping segments with a 50% overlap [*Schulz and Stattegger*, 1997; *Welch*, 1967]. The WOSA method reduces noise in the estimated spectra in exchange for reducing the frequency resolution [*Welch*, 1967]. A Blackman-Harris window was then applied to each segment prior to obtaining the Lomb-Scargle periodogram to reduce spectral leakage. The periodogram for the time series was obtained by averaging the periodograms for each segment [*Schulz and Mudelsee*, 2002]. To take into consideration the *x* and *y* uncertainty in the time series analysis, we

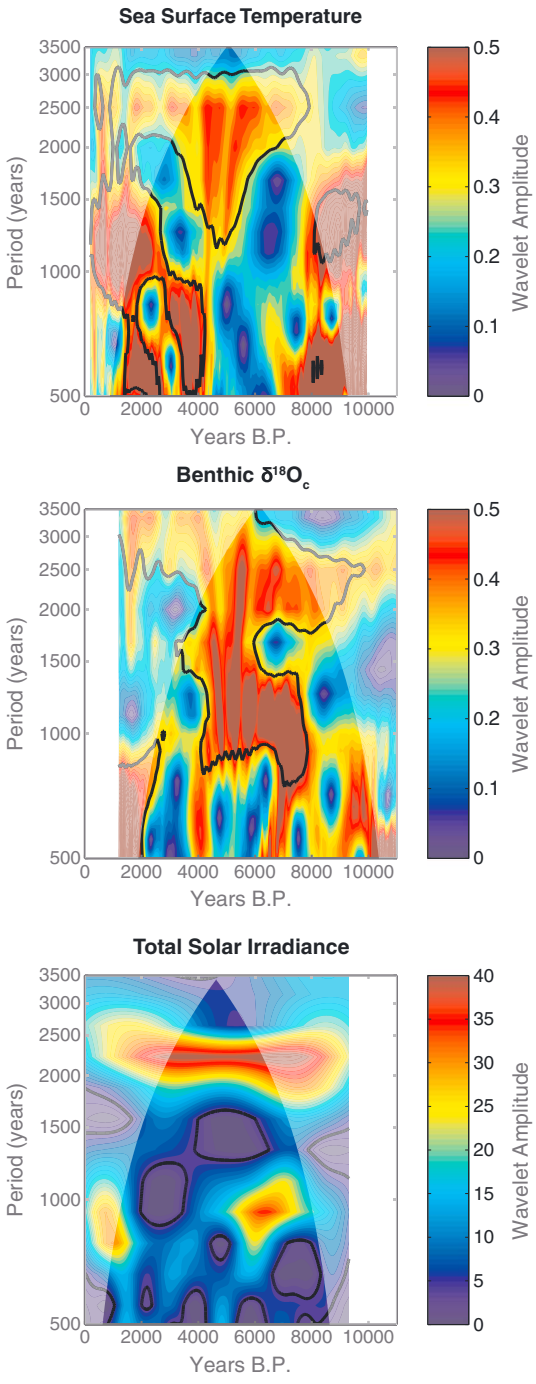

Figure 6.

also performed spectral analysis on each rendition of the time series generated through Monte Carlo simulations. The uncertainty on the spectral peaks was then expressed as the 95% envelope of the 10,000 simulations.

The significance of the spectral peaks was then tested against a red noise process using a autoregressive model of order 1 (AR1). *Robinson* [1977] showed that a discrete AR1 process r for times t_j (with $j = 1, 2, \ldots, n$) with arbitrary spacing is given by $r(t_j) = \rho_j r(t_{j-1}) + \varepsilon(t_j)$, where $\rho_j = \exp(-(t_j - t_{j-1})/T)$. The constant T is the characteristic timescale of the AR1 process and represents a measure of its memory while ε indicates "white" Gaussian noise with zero mean and variance $\sigma_\varepsilon^2 = 1 - \exp(-2(t_j - t_{j-1})/T)$. The value of T was estimated from the unevenly spaced time series using the least squares algorithm devised by *Mudelsee* [2002]. An ensemble of 1000 AR1 models was generated with a fixed T value. The significance is tested against the 50, 80, and 95 percentile of the AR1 ensemble.

To quantify the evolution of the periodicity throughout the Holocene [*Debret et al.*, 2009, 2007], we used wavelet analysis. In this study, we applied the weighted wavelet Z-transform (WWZ) for unevenly-spaced time series as described by *Foster* [1996] and implemented by *Witt and Schumann* [2005]. The WWZ algorithm is based on the abbreviated Mortlet-Wavelet $f(t) = e^{-c\omega^2(t-\theta)^2} \cdot e^{i\omega(t-\theta)}$, where ω represents the angular frequency, t is time in the times series, θ is a vector of evenly spaced time to be considered in the analysis, and c is the decay constant set here as $(8\pi^2)^{-1}$ [*Foster*, 1996; *Witt and Schumann*, 2005]. The significance was tested against an ensemble of AR1 models generated with a fixed T value, following the procedure outlined for the Lomb-Scargle periodogram.

4. Results: Tropical Pacific and Southern Ocean Variability

4.1. Tropical Pacific Sea Surface Variability Over the Holocene

The SST and $\delta^{18}O_{sw}$ records inferred from paired Mg/Ca and $\delta^{18}O_c$ measurements on *G. ruber* are presented in Figure 4. Both records are characterized by millennial-scale variability, which persisted through the Holocene. Spectral analysis (Figure 5) indicates there is enhanced variability at millennial timescales, with periodicities of ~1100 years, ~1400 years and ~2700 years in SST and ~1100 years, ~1300 years, and ~2400 years in $\delta^{18}O_{sw}$. This

millennial-scale variability is robust despite age, analytical, and calibration uncertainties (Figures 5a and 5b). The last oscillation corresponds to the Northern Hemisphere Medieval Warm Period/Little Ice Age, which has been previously documented in this region [*Newton et al*., 2006, 2011; *Oppo et al*., 2009]. Wavelet analysis of the SST record shows that although the 2500 year (and to some extent the 1500 year) periodicity is present throughout the Holocene, the 1000 year periodicity is strongest in the early (8000–10,000 years B.P.) and late (0–3000 years B.P.) Holocene (Figure 6). The amplitude of Holocene millennial-scale SST variability in the western equatorial Pacific is 0.5°C (0.4–0.8°C), inferred from the 900–3000 year band-pass filtered SST record (Figure 4). Prior to filtering, the time series was interpolated onto an evenly spaced grid, which corresponds to the age model common to all Monte Carlo realizations. The quoted uncertainty in parenthesis represents the 95% confidence interval of millennial-scale SST variability inferred from the 10,000 Monte Carlo simulations, after applying the same band-pass filter to each realization of the time series.

The amplitude of the millennial-scale $\delta^{18}O_{sw}$ is 0.22‰ (0.19–0.31‰), inferred from the 900–3000 year band-pass filtered $\delta^{18}O_{sw}$ record (Figure 4). As for SST, the quoted uncertainty is derived from the 10,000 Monte Carlo simulations. Changes in $\delta^{18}O_{sw}$ generally tracked SSTs with periods of warmer SST associated with an increase in $\delta^{18}O_{sw}$. We further explore the relationship between SST and $\delta^{18}O_{sw}$ variability over the Holocene by using 3 band-pass filters (900–1200 years, 1200–2000 years, and 2000–3000 years, Figure S1) corresponding to the spectral peaks. All these periodicities contribute to the millennial-scale signal presented in Figure 4. We determine the phase angle between the SST and $\delta^{18}O_{sw}$ record using the following relation:

$$\phi = \cos^{-1}\left(\frac{\overrightarrow{SST}.\overrightarrow{\delta^{18}O_{sw}}}{\left\|\overrightarrow{SST}\right\|\left\|\overrightarrow{\delta^{18}O_{sw}}\right\|}\right)$$

In this equation, Φ represents the phase angle, and SST and $\delta^{18}O_{sw}$ represents the band-passed time series. The uncertainty in the phase angle is assessed using the Monte-Carlo simulations. We ensure that the Monte-Carlo SST and $\delta^{18}O_{sw}$ realizations were based on the same age model since these parameters were determined on the same foraminiferal sample. The average phase angles between SST and $\delta^{18}O_{sw}$ are 37° (18°–71°), 66° (32°–93°), and 32° (11°–59°) on the 1000 year, 1500 year, and 2500 year timescale, respectively. The 95% confidence interval on the estimate of the phase angle is given in parenthesis. We can then calculate the time shift using the following equation:

$$t = \frac{\phi \times \tau}{360°}$$

where Φ represents the phase angle and τ represents the length of the cycle (either 1000 years, 1500 years, or 2500 years). The phase angles correspond to a time shift of ~100 years (50–200 years), ~250 years (130–390 years), and ~200 years (80–410 years), respectively.

4.2. Upper Circumpolar Deep Water Variability Over the Holocene

The benthic $\delta^{18}O_c$, after correction for ice volume effect [*Waelbroeck et al*., 2002], is presented in Figure 4. The benthic $\delta^{18}O_c$ record is also characterized by millennial-scale variability that persisted throughout the Holocene. Spectral analysis (Figure 5c) indicates there is enhanced millennial-scale variability within benthic $\delta^{18}O_c$ at periodicities of ~1000 years, ~1600 years and ~2500 years, similar to the periodicities identified in the planktonic SST and $\delta^{18}O_{sw}$ records. Wavelet analysis (Figure 6) confirms the presence of the 2500 year periodicity throughout the Holocene. In contrast, the 1000 and 1500 year periodicities are only significant in the mid-Holocene (4000–8000 years B.P.). The magnitude of millennial-scale $\delta^{18}O_c$ variability

Figure 6. Wavelet analysis. (top) Wavelet analysis of the SST record. The bold lines represent the 95% ensemble of the red noise (AR1) models. The AR1 models were generated using a characteristic timescale $T = 5.5$ years obtained from TAUEST [*Mudelsee*, 2002]. The shaded area represents the cone of influence. Please note that although the wavelet spectrum shows power in the 1000 and 1500 year band in the early Holocene, this power is not significant because of the resolution of the time series during this time period. (middle) Same as Figure 6 (top) but for the benthic $\delta^{18}O_c$ record. The characteristic timescale is $T = 7$ years. To take into consideration the uneven spacing of the time series, we used the technique described by *Foster* [1996]. (bottom) Wavelet analysis of the *Steinhilber et al*. [2009] TSI record using the MATLAB package developed by *Torrence and Compo* [1998] for evenly spaced time series. Note that most of the millennial timescale variability is significant, except for the 1500 year band.

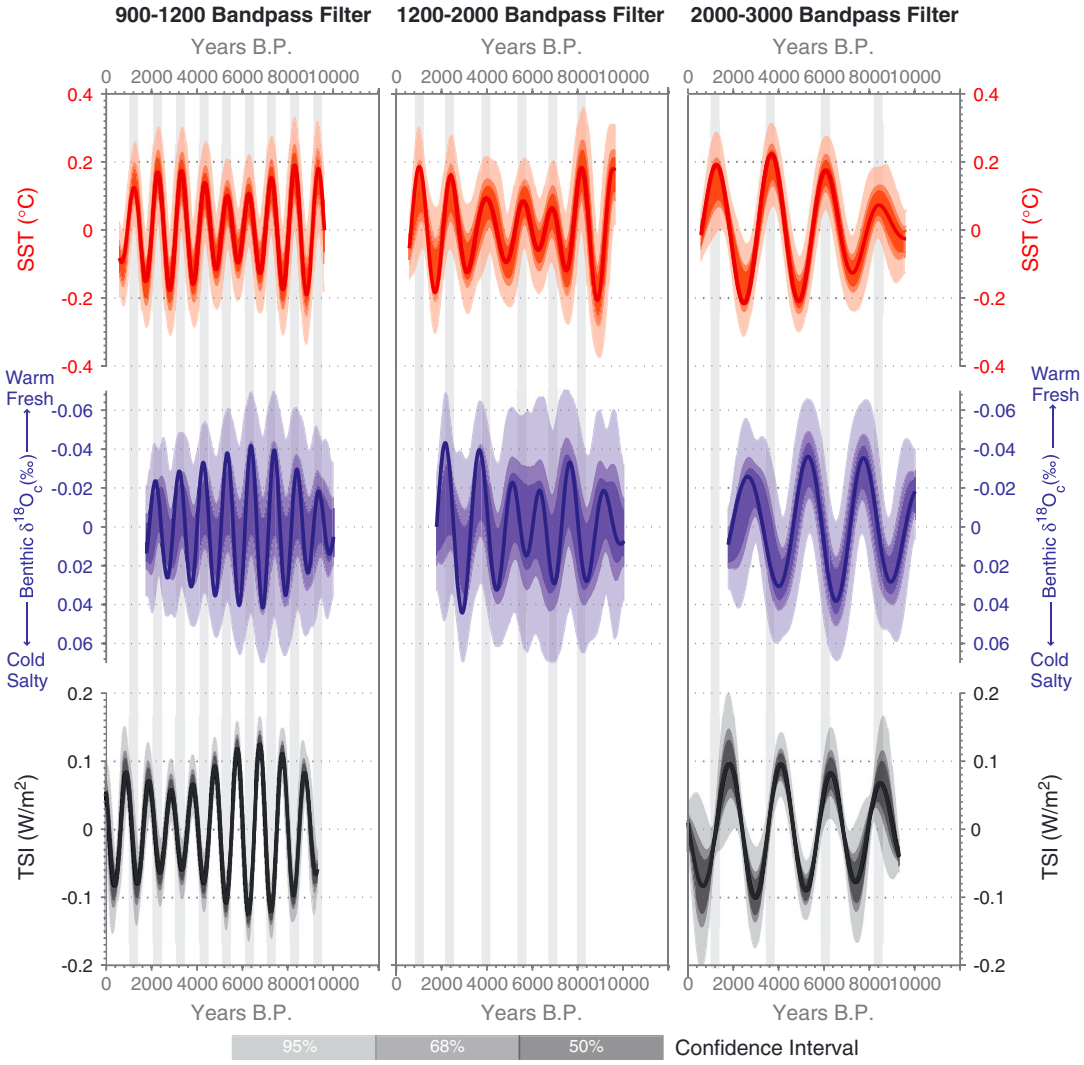

Figure 7. Tropical Pacific versus Southern Ocean variability over the Holocene. (left) The 900–1200 year band-pass record of SST (red), UCDW variability (blue), and solar variability (black). The shaded area corresponds to the 50%, 68%, and 90% confidence level on the band-pass records obtained from the 10,000 Monte Carlo simulations. The vertical lines correspond to times of higher SSTs. (middle) Same as Figure 7 (left) but for the 1200–2000 years band-pass filter. Since the solar spectrum does not show significant periodicities at this timescale, the solar band-pass filtered record is not shown. (right) Same as Figure 7 (left) but for the 2000–3000 years band-pass filter. Note that the *y* axis amplitude is the same for all filters to highlight the different amplitude of variability among the different timescales. The uncertainty on the band-pass filters was estimated for the common length of the age model as extrapolation would bias the uncertainty estimates.

is 0.10‰ (0.09–0.18‰), inferred from the 900–3000 year band-pass record (95% confidence interval in parenthesis, Figure 4).

As for the planktonic data set, we decom-posed the benthic $\delta^{18}O_c$ record using three band-pass filters to investigate the timing of SST and deep ocean temperature and salinity variability on millennial timescale during the Holocene (Figure 7). The large uncertainty associated with our estimate of transit time prevents any significant comparison with the planktonic data on the ~1000 year and ~1500 year timescales since the 1σ range age uncertainty (~600 years) represents about half a cycle. The phase angle (95% confidence interval given in parenthesis) between SST and benthic $\delta^{18}O_c$ variability is 57° (20°–139°) on the ~2500 year timescale. This corresponds to an average time shift of ~400 years (140–960 years). The relative timing of Southern Ocean and tropical Pacific variations is consistent throughout the Holocene, with UCDW warming and/or freshening lagging tropical Pacific warming by ~850 years (290–1110 years).

5. Discussion

The ~1000 year, ~1500 year, and 2500 year periodicities found in both the planktonic and benthic records of MD81 are observed in other Holocene records (for a review, *Wanner et al.* [2008]). [*Debret et al.*, 2007, 2009] assigned the 1000 year and 2500 year spectral signatures to external (solar) forcing while the 1500 year periodicity has been attributed to internal forcing, including ocean circulation and/or an ocean/atmosphere coupling [*Debret et al.*, 2009, 2007; *Denton and Broecker*, 2008]. In the following sections, we evaluate whether (1) the solar hypothesis can explain the features of the MD81 SST record and (2) whether the timing of UCDW changes coincides with changes in North Atlantic deep water variability inferred from North Atlantic proxy records.

5.1. Solar Forcing Hypothesis

We assess whether the magnitude and timing of western tropical SST are consistent with solar forcing. Spectral analysis on the global TSI record of *Steinhilber et al.* [2009] shows two significant millennial scale periodicities centered around ~1000 years and ~2500 years (Figure 5d) in agreement with previous studies [*Debret et al.*, 2009, 2007]. Wavelet analysis (Figure 6) suggests that although the 2500 year periodicity is present throughout the Holocene, the 1000 year periodicity is strongest in the mid-Holocene (6000–8000 year B.P.). Applying band-pass filters of 900–1200 years and 2000–3000 years highlights these cycles over the Holocene (Figure 7). The uncertainty in the band-passed TSI records was assessed using the same Monte-Carlo process applied to the MD81 record. The TSI values were varied within a normal distribution characterized by a standard deviation corresponding to the reported uncertainty at each horizon. Each Monte-Carlo realization was then band-pass filtered for the periodicities of interest. The TSI variability on millennial timescale is on the order of 0.2Wm^{-2} (95% confidence interval from the Monte Carlo simulations: 0.1–0.3Wm^{-2}) inferred from the band-pass records. On the ~1000 year and ~2500 year timescales, the magnitude of SST variability is 0.3 °C (95% confidence interval: 0.2–0.5°C). The climate sensitivity to solar cycles is then defined as $\lambda_{solar} = \partial T/(\varepsilon \partial F)$ [*Tung et al.*, 2008], where ∂T is the change in temperature, ∂F is the radiative forcing change and ε is the efficacy factor. ∂F is defined as $\partial S(1-\alpha)/4$, where ∂S represents TSI variability, the factor four accounts for the geometry of the Earth and $\alpha \approx 0.3$ is the average albedo of the Earth. For the definition of climate sensitivity to be broadly applicable to greenhouse gas forcing or solar cycles, the efficacy factor is introduced in the sensitivity equation and measures the ratio of a unit of radiative change due to changes in insolation to a unit of radiative change due to CO_2 [*Forster et al.*, 2007], in other words, $\varepsilon = \lambda_{solar}/\lambda_{CO2}$, where λ_{CO2} represents the climate sensitivity to CO_2. The efficacy factor for solar forcing has been calculated by several global climate models as outlined in the Intergovernmental Panel on Climate Change report (AR4) and falls within the range of 0.7–1 [*Forster et al.*, 2007]. Therefore, the range of λ_{solar} inferred from the MD81 data set is 9.3–16.7°C/Wm^{-2} for the range of efficacy factors (95% confidence interval: 5.5–32°C/Wm^{-2}). *Tung et al.* [2008] estimated a equilibrium sensitivity to the 11 year solar cycle on the order of 1–1.5°C/Wm^{-2}, an order of magnitude lower than our estimate from the MD81 record on millennial timescale. There remains the possibility that (1) the *Steinhilber et al.* [2009] reconstruction underestimate actual TSI variability and (2) the response to small changes in solar irradiance was locally enhanced in western tropical Pacific. The solar reconstruction of *Vieira et al.* [2011] show similar magnitude of TSI variability over millennial timescales as the TSI reconstruction used in this study. Therefore, possibility (1) will remain untested until other reconstructions of Holocene TSI variability become available. The study by *Tung et al.* [2008] using twentieth century reanalysis data and the modeling work of *Swingedouw et al.* [2011] both suggest a nonuniform response of the climate system to solar forcing. However, in both studies, the largest temperature changes occur at the poles rather than the tropics. It is possible that the ocean's subsurface circulation and memory on longer timescales could result in an enhanced tropical response, which were not considered in these modeling studies. Therefore, possibility (2) cannot be completely rejected at this time. Furthermore, the wavelet analysis and the amplitude changes observed in the band pass-filtered records suggest a highly nonlinear-response of tropical SSTs to TSI changes. Wavelet analysis suggests enhanced tropical SSTs variability in the early and late Holocene, an observation supported by increased amplitude in the band pass-filtered record. On the other hand, the amplitude of TSI changes is highest in the mid-Holocene when SST variability is low (Figure 7).

We then consider the response time of the tropical Pacific to TSI changes. The phase angles between the MD81 planktonic record and the TSI reconstruction of *Steinhilber et al.* [2009] are 144° (93°–153°) and 64° (30°–97°) on the 1000 year and 2500 year timescales, respectively. We first considered that this different phasing

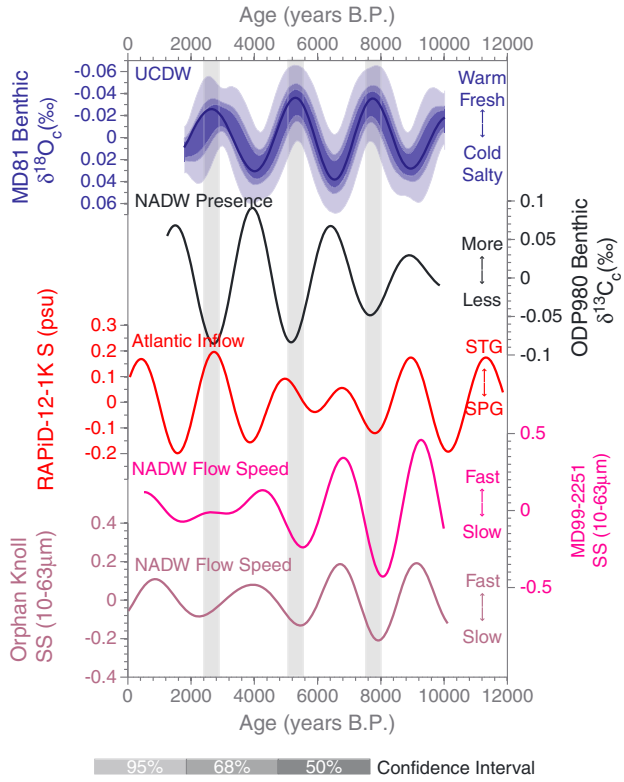

Figure 8. Southern Ocean versus North Atlantic variability. All records were band-passed at 2000–3000 years to highlight variability on this timescale. UCDW variability (blue) over the Holocene inferred from benthic foraminifera $\delta^{18}O_c$. The shaded area corresponds to the 50%, 68%, and 90% confidence level on the band-pass record obtained from the 10,000 Monte Carlo simulations. The uncertainty on the band-pass filter was estimated for the common length of the age model as extrapolation would bias the uncertainty estimates. ODP site 980 (black) benthic foraminifera $\delta^{13}C$ taken to represent the proportion of NADW and southern-sourced water at this site. Subsurface salinity record (red) obtained from paired Mg/Ca and $\delta^{18}O$ on the planktonic foraminifer G. inflata, taken to represent the proportion of cold, fresh subpolar water and warm, salty subtropical water in the Atlantic Inflow. Mean grain size sortable silt fraction in the Gardar Drift (MD99-2251, pink) and Orphan Knoll (purple) representing the flow speed of NADW. The vertical shaded areas represent periods of low benthic $\delta^{18}O_c$ in the MD81 record, associated with warmer/fresher surface conditions in the Southern Ocean.

could be attributed to age model uncertainty. To test this hypothesis, we created two new age models for the MD81 planktonic record, which would allow for a similar response of the tropical Pacific to TSI changes. The new age models were constructed by associating periods of high (low) SSTs with periods high TSI on both timescales (Figure S2). Doing so not only creates age model reversals through the record but also requires the new age models to be outside of the 95% confidence interval defined from the ^{14}C measurements. We therefore conclude that our result is robust and not an artifact of the age model. Despite the difference in phasing, the response time of SST to solar forcing is ~400 years on both the 1000 year and 2500 year timescales (95% confidence interval: 260–450 years on the 1000 year timescale and 210–670 years on the 2500 year timescale). In other words, the peak warming in the western tropical Pacific occurs 400 years after the peak in TSI on both timescales. The possibility that the observations results from an integration of effects over multiple centuries is intriguing and supported by modeling studies [*Hewitt et al.*, 2003; *Stouffer*, 2004]. A long integration time of effect may potentially explain the high climate sensitivity inferred from our record as the deep ocean may act as an amplifier by way of integrating to forcing and altering circulation strengths at out core location. However, this also implies a sizable response of deep water circulation in response to what is likely a fairly small signal in surface climate. Therefore, although we cannot totally discount the possibility that solar forcing is the source of the 1000 year and 2500 year SST variability observed in the MD81 record, we do not find the evidence particularly compelling. In the following sections, we also investigate alternative, but not necessarily mutually exclusive, hypotheses.

5.2. Internal Forcing Hypothesis

We present alternative hypotheses for forced or unforced modes of variability within the climate system. We first consider that these periodicities arise from internal, unforced processes within the climate system. A modeling study by *Hunt* [2006] demonstrated that an unforced climatic system could not sustain the long-term climatic anomalies associated with the Medieval Climate Anomaly and the Little Ice Age over a majority of the oceans and the Southern Hemisphere. In contrast, *Karnauskas et al.* [2012] identified internal centennial-scale variability of ~0.5°C in the western tropical Pacific in long control integrations a fully coupled global climate models. Considering the importance of the IPWP to the global climate system, the question as to whether these SST anomalies could be sustained on the longer timescales which are the focus of the present study deserves further investigation.

We then investigate whether the forced response of the climate system involves deep ocean changes. Paleoceanographic data from the North Atlantic [*Bianchi and McCave*, 1999; *Giraudeau et al*., 2000; *Hoogakker et al*., 2011; *Oppo et al*., 2003; *Thornalley et al*., 2009] and modeling studies [*Delworth and Zeng*, 2012; *Hofer et al*., 2011; *Miller et al*., 2012] suggest that variations in the configuration of North Atlantic deep water masses and in the strength of the Atlantic Meridional Overturning Circulation (AMOC) are possible under Holocene boundary conditions. In this section, we address whether changes in deep water mass variability inferred from four proxy records from the North Atlantic [*Hoogakker et al*., 2011; *Oppo et al*., 2003; *Thornalley et al*., 2009] coincided with changes in Southern Ocean variability inferred from the MD81 benthic $\delta^{18}O_c$ record. Spectral analysis of these records (Figure S3) shows significant millennial-scale periodicities during the Holocene similar to the MD81 benthic $\delta^{18}O$ spectrum. To explore the relationship between the North Atlantic and MD81 benthic records, we band-passed the North Atlantic records at 2000–3000 years (Figure 8). We forgo analysis on the ~1000 year and ~1500 year timescale since the uncertainty in the benthic MD81 record prevents any significant comparisons. On the 2500 year timescale, periods of warm and/or fresh Southern Ocean are associated with (1) an increase in the proportion of low-density subpolar water relative to higher-density subtropical gyre water to the Atlantic inflow, which represents the surface limb of AMOC [*Thornalley et al*., 2009], (2) a decrease in the flow speed of North Atlantic Deep water [*Hoogakker et al*., 2011], and (3) an increase in southern-sourced water at site (ODP980 980, 55°N, 15°W, 2179 m), which is presently bathed by NADW (Figure 8). These records suggest a role for the deep ocean in Holocene millennial-scale variability, perhaps in combination with solar forcing or as a means to sustain unforced temperature anomalies observed in some models on centennial timescale [*Karnauskas et al*., 2012].

We also consider volcanoes as a possible forcing. Volcanoes provide a source of randomness that could produce power at longer timescales. Here we propose a simple red noise model to test whether the frequency and amplitude of volcanic eruptions during the Holocene could explain our tropical SST reconstruction. The red noise process for times t_j, evenly spaced at 5 year intervals, is: $r(t_j) = \gamma r(t_{j-1}) + \varepsilon(t_j) + \xi(t_j)$, where γ is the lag-1 autocorrelation and represents a measure of the memory of the system, ε indicates "white" Gaussian noise with mean and variance equal to those of the Community Climate System Model, version 4 (CCSM4) control simulation ($\sigma_\varepsilon = 0.1$°C), and ξ represents the volcanic forcing (in degree Celsius) at time t_j. The volcanic forcing was inferred from the volcanic sulfate flux measured in an Antarctic ice core [*Castellano et al*., 2005], normalized relative to the sulfate flux associated with Mount Pinatubo eruption. Volcanic sulfate concentrations recorded in Greenland ice suggest a higher frequency of volcanic events throughout the Holocene; a difference attributed to the relative closeness of Greenland to areas with a high density of active volcanoes [*Castellano et al*., 2005]. However, how these high-latitude eruptions would affect tropical climate variability is unclear, and we therefore use the Antarctic estimates. We then need to assign a tropical Pacific response to the volcanic eruptions. *Frölicher et al*. [2013] estimated the tropical Pacific cooling within 4 years of Mount Pinatubo eruption to be −0.3°C. This sensitivity is used to assign a cooling amplitude using a linear transfer function to the eruptions recorded in the Antarctic ice core through the Holocene. We compared our results to a red noise model without the volcanic forcing ($r(t_j) = \gamma r(t_{j-1}) + \varepsilon(t_j)$). Our simple red noise model is able to reproduce the shape of the MD81 SST spectrum with very specific peaks and power gaps in-between these peaks (Figure S4). However, the amplitude of simulated tropical Pacific variability depends on both the value of γ and the volcanic forcing. Without volcanic forcing, it is impossible to simulate the correct amplitude of western tropical Pacific SST variability over the Holocene (Figure S5). We estimated the lag-1 autocorrelation coefficient (γ) from the CCSM4 control simulation to be between 0.1 and 0.3 within IPWP. For this value of γ, simulated tropical SST variability is on the order of 0.2°C (Figure S5). To get the full response (~0.5°C), we need to increase γ to ~0.9. Increasing either the frequency of Holocene volcanic events or the temperature amplitude response to volcanic events cannot reproduce the observed SST variability. Possible combination of amplitude/frequency and γ could make this hypothesis possible. While volcanoes may present an explanation for the inferred Holocene millennial-scale variability in MD81, our simple red noise model requires an implausibly high memory ($\gamma = 0.9$), higher amplitude or more frequent forcing than we have presumed. It is conceivable that the ocean's subsurface circulation and memory can create a larger red noise process memory on longer timescales. Thus, we do not want to totally discount this hypothesis; however, our simple calculation suggests it is not likely to work out. An alternate hypothesis that the origin for millennial-scale variability lies in the climate system itself either as a self-sustaining mode or a mode excited by a large-scale perturbation to the climate system such as the deglaciation, in which the timescale is controlled by ocean basin characteristic and/or boundary conditions [*Alley et al*., 2001; *Marchal*

et al., 2007; *Sakai and Peltier*, 1997; *Schulz*, 2002; *Timmermann et al*., 2003]. A full assessment of whether stochastic resonance could explain the MD81 Holocene record is beyond the scope of the current study although it should be taken into consideration in future studies that attempt to explain millennial-scale variability over the Holocene. Furthermore, the MD81 benthic record together with proxy records from the North Atlantic suggest that the forcing responsible for Holocene millennial-scale variability was transmitted and perhaps amplified though the deep ocean.

Acknowledgments
The authors would like to thank Miguel Rincon (University of Southern California) for helping with the analyses and John Southon (University of California Irvine) for the AMS measurements. This work was supported by two National Science Foundation grants to Stott: AGS#1049238 and AGS#1344514. Khider was funded by the USC William M. Keck Foundation Endowed Graduate Fellowship and the University of Texas Institute for Geophysics Postdoctoral Fellowship.

References

Alley, R. B., S. Anandakrishnan, and P. Jung (2001), Stochastic resonance in the North Atlantic, *Paleoceanography*, *16*(2), 190–198.
Anand, P., H. Elderfield, and M. H. Conte (2003), Calibration of Mg/Ca thermometry in planktonic foraminifera from a sediment trap time series, *Paleoceanography*, *18*(2), 1050, doi:10.1029/2002PA000846.
Antonov, J. I., D. Seidov, T. P. Boyer, R. A. Locarnini, A. V. Mishonov, and H. E. Garcia (2010), *World Ocean Atlas 2009*, Salinity, vol. 2, pp. 184, U.S. Government Printing Office, Washington, D. C.
Arbuszewski, J., P. DeMenocal, A. Kaplan, and E. C. Farmer (2010), On the fidelity of shell-derived $\delta^{18}O_{seawater}$ estimates, *Earth Planet. Sci. Lett.*, *300*, 186–196.
Barker, S., M. Greaves, and H. Elderfield (2003), A study of cleaning procedures used for foraminiferal Mg/Ca paleothermometry, *Geochem. Geophys. Geosyst.*, *4*(9), 8407, doi:10.1029/2003GC000559.
Bemis, B. E., H. J. Spero, J. Bijma, and D. W. Lea (1998), Reevaluation of the oxygen isotopic composition of planktonic foraminifera: Experimental results and revised paleotemperature equations, *Paleoceanography*, *13*(2), 150–160.
Bianchi, G. G., and I. N. McCave (1999), Holocene periodicity in North Atlantic climate and deep-ocean flow south of Iceland, *Nature*, *397*(6719), 515–517.
Bolstad, W. (2010), *Understanding Computational Bayesian Statistics*, John Wiley, Hoboken, New Jersey.
Bond, G., W. Showers, M. Cheseby, R. Lotti, P. Almasi, P. deMenocal, P. Priore, H. Cullen, I. Hajdas, and G. Bonani (1997), A pervasive millennial-scale cycle in North Atlantic Holocene and glacial climates, *Science*, *278*(5341), 1257–1266.
Bond, G., B. Kromer, J. Beer, R. Muscheler, M. N. Evans, W. Showers, S. Hoffmann, R. Lotti-Bond, I. Hajdas, and G. Bonani (2001), Persistent solar influence on North Atlantic climate during the Holocene, *Science*, *294*(2130), 2130–2136.
Broecker, W. S. (2000), Was a change in thermohaline circulation responsible for the Little Ice Age?, *Proc. Natl. Acad. Sci. U.S.A.*, *97*(4), 1339–1342.
Broecker, W. S. (2001), Was the Medieval Warm Period Global?, *Science*, *291*(5508), 1497–1499.
Cane, M. (1998), A role for the Tropical Pacific, *Science*, *282*, 59–61.
Carton, J. A., and B. S. Giese (2008), A reanalysis of ocean climate using Simple Ocean Data Assimilation (SODA), *Mon. Weather Rev.*, *136*, 2999–3017.
Castellano, E., S. Becagli, M. Hansson, M. Hutterli, J. R. Pettit, M. R. Rampino, M. Severi, J. P. Steffensen, R. Traversi, and R. Udisti (2005), Holocene volcanic history as recorded in the sulfate stratigraphy of the European Project for Ice Coring in Antarctica Dome C (EDC96) ice core, *J. Geophys. Res.*, *110*, D06114, doi:10.1029/2004JD005259.
Dannenmann, S., B. K. Linsley, D. W. Oppo, Y. Rosenthal, and L. Beaufort (2003), East Asian monsoon forcing of suborbital variability in the Sulu Sea during Marine Isotope Stage 3: Link to Northern Hemisphere climate, *Geochem. Geophys. Geosyst.*, *4*(1), 1001, doi:10.1029/2002GC000390.
Debret, M., V. Bout-Roumazeilles, F. Grousset, M. Desmet, J. F. McManus, N. Massel, D. Sebag, J. R. Petit, Y. Copard, and A. Trentesaux (2007), The origin of the 1500-year climate cycles in Holocene North Atlantic record, *Clim. Past Discuss.*, *3*, 679–692.
Debret, M., D. Sebag, X. Crosta, N. Massei, J. R. Petit, E. Chapron, and V. Bout-Roumazeilles (2009), Evidence from wavelet analysis for a mid-Holocene transition in global climate forcing, *Quat. Sci. Rev.*, *28*(25-26), 2675–2688.
Dekens, P. S., D. W. Lea, D. K. Pak, and H. J. Spero (2002), Core top calibration of Mg/Ca in the tropical foraminifera: Refining paleotemperature estimation, *Geochem. Geophys. Geosyst.*, *3*(4), 1022, doi:10.1029/2001GC000200.
Delworth, T. L., and F. Zeng (2012), Multicentennial variability of the Atlantic meridional overturning circulation and its climatic influence in a 4000 year simulation of the GFDL CM2.1 climate model, *Geophys. Res. Lett.*, *39*, L13702, doi:10.1029/2012GL052107.
Denton, G. H., and W. S. Broecker (2008), Wobbly ocean conveyor circulation during the Holocene?, *Quat. Sci. Rev.*, *27*, 1939–1950.
Forster, P., et al. (2007), Changes in atmospheric constituents and in radiative forcing, in *Climate Change 2007: The Physical Science Basis. Contribution of Working Group I to the Fourth Assessment Report of the Intergovernmental Panel on Climate Change*, edited by S. Solomon et al., pp. 197–199, Cambridge Univ. Press, Cambridge, United Kingdom and New York.
Foster, G. (1996), Wavelets for period analysis of unevenly sampled time series, *Astron. J.*, *112*(4), 1709–1729.
Frölicher, T. L., F. Joos, C. C. Raible, and J. L. Sarmiento (2013), Atmospheric CO_2 response to volcanic eruptions: The role of ENSO, season, and variability, *Global Biogeochem. Cycles*, *27*, 239–251, doi:10.1002/gbc.20028.
Ghil, M., et al. (2002), Advanced spectral methods for climatic time series, *Rev. Geophys.*, *40*(1), 1003, doi:10.1029/2000RG000092.
Giraudeau, J., M. Cremer, S. Manthé, L. Labeyrie, and G. Bond (2000), Coccolith evidence for instabilities in surface circulation south of Iceland during Holocene times, *Earth Planet. Sci. Lett.*, *179*, 257–268.
Gordon, A. L. (2005), Oceanography of the Indonesian Seas and their throughflow, *Oceanography*, *18*(4), 14–27.
Haigh, J. D. (2001), Climate variability and the influence of the Sun, *Science*, *294*(5549), 2109–2111.
Haigh, J. D. (2007), The Sun and the Earth's climate, *Living Rev. Sol. Phys.*, *4*(2), pp. 1–25.
Hewitt, C. D., R. J. Stouffer, A. J. Broccoli, J. F. B. Mitchell, and P. J. Valdes (2003), The effect of ocean dynamics in a coupled GCM simulation of the last Glacial Maximum, *Clim. Dyn.*, *20*, 203–218.
Hofer, D., C. C. Raible, and T. F. Stocker (2011), Variations of the Atlantic meridional overturning circulation in control and transient simulations of the last millennium, *Clim. Past*, *7*(1), 133–150.
Hoogakker, B. A. A., M. R. Chapman, I. N. McCave, C. Hillaire-Marcel, C. R. W. Ellison, I. R. Hall, and R. J. Telford (2011), Dynamics of North Atlantic Deep Water masses during the Holocene, *Paleoceanography*, *26*, PA4214, doi:10.1029/2011PA002155.
Hunt, B. G. (2006), The Medieval Warm Period, the Little Ice Age and simulated climatic variability, *Clim. Dyn.*, *27*(7-8), 677–694.
Jansen, E., et al. (2007), Paleoclimate, in *Climate Change 2007: The Physical Science Basis. Contribution of Working Group I to the Fourth Assessment Report of the Intergovernmental Panel on Climate Change*, edited by S. Solomon et al., pp. 463, Cambridge Univ. Press, Cambridge, United Kingdom and New York.

Jochum, M., and J. Potemra (2008), Sensitivity of tropical rainfall to Banda Sea diffusivity in the Community Climate System Model, *J. Clim.*, *21*, 6445–6454.
Karnauskas, K. B., J. E. Smerdon, R. Seager, and J. F. González-Rouco (2012), A Pacific Centennial Oscillation predicted by coupled GCMs*, *J. Clim.*, *25*(17), 5943–5961.
Key, R. M., A. Kozyr, C. Sabine, K. Lee, R. Wanninkhof, J. L. Bullister, R. A. Feely, F. J. Millero, C. Mordy, and T.-H. Peng (2004), A global ocean carbon climatology: Results from Global Data Analysis Project (GLODAP), *Global Biogeochem. Cycles*, *18*, GB4031, doi:10.1029/2004GB002247.
Kisakürek, B., A. Eisenhauer, F. Böhm, D. Garbe-Schönberg, and J. Erez (2008), Controls on shell Mg/Ca and Sr/Ca in cultured planktonic foraminiferan, *Globigeriniodes ruber* (white), *Earth Planet. Sci. Lett.*, *273*, 260–269.
Levi, C., L. Labeyrie, F. Bassinot, F. Guichard, E. Cortijo, C. Waelbroeck, N. Caillon, J. Duprat, T. De Garidel-Thoron, and H. Elderfield (2007), Low-latitude hydrological cycle and rapid climate changes during the last deglaciation, *Geochem. Geophys. Geosyst.*, *8*, Q05N12, doi:10.1029/2006GC001514.
Linsley, B. K., Y. Rosenthal, and D. W. Oppo (2010), Holocene evolution of the Indonesian throughflow and the western Pacific warm pool, *Nat. Geosci.*, *3*, 578–583.
Locarnini, R. A., A. V. Mishonov, J. I. Antonov, T. P. Boyer, and H. E. Garcia (2010), *World Ocean Atlas*, Temperature, vol. 1, pp. 184, U.S. Government Printing Office, Washington, D. C.
Lomb, N. R. (1976), Least-squares frequency analysis of unequally spaced data, *Astrophys. Space Sci.*, *39*, 447–462.
Marchal, O., C. Jackson, J. Nilsson, A. Paul, and T. F. Stocker (2007), Buoyancy-driven flow and nature of vertical mixing in a zonally averaged model, in *Ocean Circulation: Mechanisms and Impacts*, edited by A. Schmittner, J. C. H. Chiang, and S. R. Hemming, pp. 33–52, AGU, Washington D. C.
Mathien-Blard, E., and F. Bassinot (2009), Salinity bias on the foraminifera Mg/Ca thermometry: Correction procedure and implications for past ocean hydrographic reconstructions, *Geochem. Geophys. Geosyst.*, *10*, Q12011, doi:10.1029/2008GC002353.
Mayewski, P. A., et al. (2004), Holocene climate variability, *Quat. Res.*, *62*(3), 243–255.
McBride, J. L., M. R. Haylock, and N. Nichols (2003), Relationships between the maritime continent heat source and the El Niño–Southern Oscillation phenomenon, *J. Clim.*, *16*, 2905–2914.
McGregor, H. V., M. K. Gagan, M. T. McCulloch, E. Hodge, and G. Mortimer (2008), Mid-Holocene variability in the marine 14C reservoir age for northern coastal Papua New Guinea, *Quat. Geochronol.*, *3*(3), 213–225.
deMenocal, P., J. Ortiz, T. Guilderson, and M. Sarnthein (2000), Coherent high- and low-latitude climate variability during the Holocene warm period, *Science*, *288*(5474), 2198–2202.
Miller, G. H., et al. (2012), Abrupt onset of the Little Ice Age triggered by volcanism and sustained by sea ice/ocean feedbacks, *Geophys. Res. Lett.*, *39*, L02708, doi:10.1029/2011GL050168.
Monnin, E., A. Indermühle, A. Dallenbach, J. Fluckiger, B. Stauffer, T. F. Stocker, D. Raynaud, and J. M. Barnola (2001), Atmospheric CO_2 concentrations over the last glacial termination, *Science*, *291*(5501), 112–114.
Mudelsee, M. (2002), TAUEST: A computer program for estimating persistence in unevenly spaced weather/climate time series, *Comput. Geosci.*, *28*, 69–72.
Neale, R. B., and J. M. Slingo (2003), The maritime continent and its role in the global climate: A GCM study, *J. Clim.*, *16*, 834–848.
Newton, A., R. Thunell, and L. Stott (2006), Climate and hydrographic variability in the Indo-Pacific Warm Pool during the last millennium, *Geophys. Res. Lett.*, *33*, L19710, doi:10.1029/2006GL027234.
Newton, A., R. Thunell, and L. Stott (2011), Changes in the Indonesian Throughflow during the past 2000 yr, *Geology*, *39*(1), 63–66.
O'Brien, S. R., P. A. Mayewski, L. D. Meeker, D. A. Meese, M. S. Twickler, and S. I. Whitlow (1995), Complexity of Holocene climate as reconstructed from a Greenland Ice Core, *Science*, *270*(5244), 1962–1964.
Oppo, D. W., J. F. McManus, and J. L. Cullen (2003), Deepwater variability during the Holocene epoch, *Nature*, *422*, 277–278.
Oppo, D. W., Y. Rosenthal, and B. K. Linsley (2009), 2,000-year-long temperature and hydrology reconstructions from the Indo-Pacific warm pool, *Nature*, *460*, 1113–1116.
Polissar, P. J., M. B. Abbott, A. P. Wolfe, M. Bezada, V. Rull, and R. S. Bradley (2006), Solar modulation of Little Ice Age climate in the tropical Andes, *Proc. Natl. Acad. Sci. U. S. A.*, *103*(24), 8937–8942.
Qu, T., Y. Du, J. Strachan, G. Meyers, and J. Slingo (2005), Sea surface temperature and its variability in the Indonesian region, *Oceanography*, *18*(4), 50–61.
Regenberg, M., D. Nurnberg, S. Steph, J. Groeneveld, D. Garbe-Schonberg, R. Tiedemann, and W.-C. Dullo (2006), Assessing the effect of dissolution on planktonic foraminiferal Mg/Ca ratios: Evidence from Caribbean core tops, *Geochem. Geophys. Geosyst.*, *7*, Q07P15, doi:10.1029/2005GC001019.
Reimer, P. J., et al. (2009), Intcal09 and Marine09 radiocarbon age calibration curves, 0–50,000 years cal BP, *Radiocarbon*, *51*(4), 1111–1150.
Rintoul, S. R., S. Sokolov, and J. A. Church (2001), *Ocean Circulation and Climate. Observing and Modelling the Global Ocean*, Academic Press, London.
Robinson, P. M. (1977), Estimation of a time series model from unequally spaced data, *Stochastic Processes Appl.*, *6*, 9–24.
Saikku, R., L. Stott, and R. Thunell (2009), A bi-polar signal recorded in the western tropical Pacific: Northern and Southern Hemisphere climate records from the Pacific warm pool during the last Ice Age, *Quat. Sci. Rev.*, *26*(23-24), 2374–2385.
Sakai, K., and W. R. Peltier (1997), Dansgaard-Oeschger Oscillations in a coupled atmosphere-ocean climate model, *J. Clim.*, *10*, 949–970.
Scargle, J. D. (1982), Studies in astronomical time series analysis. II. Statistical aspects of spectral analysis of unevenly spaced data, *Astrophys. J.*, *263*(2), 835–853.
Scargle, J. D. (1989), Studies in astronomical time series analysis. III. Fourier transforms, autocorrelation functions, and cross-correlation functions of unevenly spaced data, *Astrophys. J.*, *343*(2), 874–887.
Schulz, M. (2002), Relaxation oscillators in concert: A framework for climate change at millennial timescales during the late Pleistocene, *Geophys. Res. Lett.*, *29*(24), 2193, doi:10.1029/2002GL016144.
Schulz, M., and M. Mudelsee (2002), REDFIT: Estimating red-noise spectra directly from unevenly spaced paleoclimatic time series, *Comput. Geosci.*, *28*, 421–426.
Schulz, M., and K. Stattegger (1997), SPECTRUM: Spectral analysis of unevenly spaced time series, *Comput. Geosci.*, *23*(9), 929–945.
Sikes, E. L., C. R. Samson, T. P. Guilderson, and W. R. Howard (2000), Old radiocarbon ages in the southwest Pacific Ocean during the last glacial period and deglaciation, *Nature*, *405*, 555–559.
Skinner, L. C., and I. N. McCave (2003), Analysis and modelling of gravity- and piston coring based on soil mechanics, *Mar. Geol.*, *199*, 181–204.
Southon, J., M. Kashgarian, M. R. Fontugne, B. Metivier, and W. W.-S. Yim (2002), Marine reservoir corrections for the Indian Ocean and southeast Asia, *Radiocarbon*, *44*(1), 167–180.

Steinhilber, F., J. Beer, and C. Fröhlich (2009), Total solar irradiance during the Holocene, *Geophys. Res. Lett.*, *36*, L19704, doi:10.1029/2009GL040142.
Stott, L., C. Poulsen, S. Lund, and R. Thunell (2002), Super ENSO and global climate oscillations at millennial time scales, *Science*, *297*(5579), 222–226.
Stott, L., K. Cannariato, R. Thunell, G. H. Haug, A. Koutavas, and S. Lund (2004), Decline of surface temperature and salinity in the western tropical Pacific Ocean in the Holocene epoch, *Nature*, *431*, 56–59.
Stott, L., A. Timmermman, and R. Thunell (2007), Southern Hemisphere and Deep-Sea Warming led to deglacial atmospheric CO_2 rise and tropical warming, *Science*, *318*, 435–438.
Stouffer, R. J. (2004), Time scales of climate response, *J. Clim.*, *17*, 209–217.
Swingedouw, D., L. Terray, C. Cassou, A. Voldoire, D. Salas-Melia, and J. Servonnat (2011), Natural forcing of climate during the last millennium: Fingerprint of solar variability. Low frequency solar forcing and NAO, *Clim. Dyn.*, *36*, 1349–1364.
Thornalley, D. J. R., H. Elderfield, and I. N. McCave (2009), Holocene oscillations in temperature and salinity of the surface subpolar North Atlantic, *Nat. geosci.*, *457*, 711–714.
Timmermann, A., H. Gildor, M. Schulz, and E. Tziperman (2003), Coherent resonant millennial-scale climate oscillations triggered by massive meltwater pulses, *J. Clim.*, *16*, 2569–2585.
Torrence, C., and G. P. Compo (1998), A practical guide to wavelet analysis, *Bull. Am. Meteorol. Soc.*, *79*, 61–78.
Tung, K. K., J. Zhou, and C. D. Camp (2008), Constraining model transient climate response using independent observations of solar-cycle forcing and response, *Geophys. Res. Lett.*, *35*, L17707, doi:10.1029/2008GL034240.
van de Flierdt, T., M. Frank, A. N. Halliday, J. R. Hein, B. Hattendorf, D. Gunther, and P. W. Kubik (2004), Deep and bottom water export from the Southern Ocean to the Pacific over the past 38 million years, *Paleoceanography*, *19*, PA1020, doi:10.1029/2003PA000923.
Viau, A. E., K. Gajewski, P. Fines, D. E. Atkinson, and M. C. Sawada (2002), Widespread evidence of 1500 year climate variability in North America during the past 14,000 year, *Geology*, *30*(5), 455–458.
Vieira, L. E. A., S. K. Solanki, N. A. Krivova, and I. Usoskin (2011), Evolution of the solar irradiance during the Holocene, *Astron. Astrophys.*, *531*(A6), 20, doi:10.1051/0004-6361/201015843.
Waelbroeck, C., L. Labeyrie, E. Michel, J. C. Duplessy, J. F. McManus, K. Lambeck, E. Balbon, and M. Labracherie (2002), Sea level and deep water temperature changes derived from benthic foraminifera isotopic records, *Quat. Sci. Rev.*, *21*, 295–305.
Wang, Y., H. Cheng, R. L. Edwards, Y. He, X. Kong, Z. An, J. Wu, M. J. Kelly, C. A. Dykoski, and X. Li (2005), The Holocene Asian monsoon: Links to solar changes and North Atlantic Climate, *Science*, *308*(5723), 854–857.
Wanner, H., et al. (2008), Mid- to Late Holocene climate change: An overview, *Quat. Sci. Rev.*, *27*(19-20), 1791–1828.
Welch, P. D. (1967), The use of Fast Fourier transform for the estimation of power spectra: A method based on time averaging over short, modified periodograms, *IEEE Trans. Audio Electroacoust.*, *15*(2), 70–73.
Wilks, D. S. (2011), *Statistical Methods in the Atmospheric Sciences*, 3rd ed., pp. 676 , Elsevier, United States.
Witt, A., and A. Y. Schumann (2005), Holocene climate variability on millennial scales recorded in Greenland ice cores, *Nonlinear Processes Geophys.*, *12*, 345–352.
Xu, J., A. Holbourn, W. Kuhnt, Z. Jian, and H. Kawamura (2008), Changes in the thermocline structure of the Indonesia outflow during Terminations I and II, *Earth Planet. Sci. Lett.*, *273*, 152–162.
Yoneda, M., H. Uno, Y. Shibata, R. Suzuki, Y. Kumamoto, K. Yoshida, T. Sasaki, A. Suzuki, and H. Kawahata (2007), Radiocarbon marine reservoir ages in the western Pacific estimated by pre-bomb molluscan shells, *Nucl. Instrum. Methods Phys. Res. Sect. B*, *259*, 432–437.